Supporting Information

Regioselective Oxidative Bromination of Arenes by Metal-Organic Framework Confined Mono-Bipyridyl Iron(III) Catalyst

Rahul Kalita,†[a] Aditya Kumar,†[a] Poorvi Gupta,[a] Bharti Rana,[a] Bitan Sardar,[a] Manav Chauhan,[a] Biplab Ghosh,[b] Yukti Monga,*[c] and Kuntal Manna*[a]

[a]Department of Chemistry, Indian Institute of Technology Delhi, Hauz Khas, New Delhi 110016, India

[b]BARC Beamlines Section, Indus-2, RRCAT, Indore 452013, India

[c]Shyamlal College, Department of Chemistry, University of Delhi, Delhi, 110032, India,

*Email: kmanna@chemistry.iitd.ac.in.

Table of contents

1. General experiment.

All the experiments were performed under an air atmosphere in a Schlenk tube, except if any case was demonstrated.

1.1. Solvents and Reagents.

All the solvents were purchased from Finar and used without further purification. All the reagents are commercially available and used directly as received. Trifluoracetic acid (TFA) was purchased from Central Drug House Pvt. Ltd. (CDH Chemicals), $KMnO_4$ was purchased from Merck, and $FeCl_3.6H_2O$ and $ZrCl_4$ were purchased from Sigma Aldrich. [2,2’-Bipyridine]-5,5’-dicarboxylic acid was synthesised from 5,5’-dimethyl-2,2’-bipyridine modifying the reported procedure.[1] 5,5’-Dimethyl-2,2’ bipyridyl was purchased from TCI.

1.2. Instrumentation.

Nuclear magnetic resonance (NMR) spectra were recorded on a Bruker NMR 500 DRX spectrometer at 500 MHz and referenced to the proton resonance resulting from $CDCl_3$ (δ 7.26) and DMSO-d_6 (δ 2.5).

Thermogravimetric analysis (TGA) was performed on a PerkinElmer TGA7 system on well-ground samples in a flowing nitrogen atmosphere with a heating rate of 10 °C/min and a 40-800 °C range.

Powder X-ray diffraction (PXRD) data were collected on a Bruker Advance diffractometer using Ni-filtered Cu Kα radiation (λ= 1.5406 Å). Data were collected with a step size of 0.05° and at count time of 1s per step over the range $4° < 2\theta < 70°$. The experimental and simulated PXRD patterns are in good agreement, indicating the bulk samples' monophasic nature. The moist sample was mounted on a PXRD groove for powder X-ray diffraction measurement of MOFs. After catalysis, bpy-UiO-Fe MOF was recovered after centrifugation and stored in THF. Just before the PXRD measurement, the THF was removed, and the moist sample was mounted on a PXRD groove. The catalysis was carried out without any mechanical stirring, and the recovered MOF was not dried before the measurement of PXRD to prevent any mechanical degradation and pore collapse of the MOF.

Inductively coupled plasma optical emission spectroscopy (ICP-OES) data were obtained with an Agilent 5110 ICP-OES and analysed using Dichroic Spectral Combiner (DSC). Samples were diluted in a 5% HNO_3 matrix and analysed with a six-point standard curve over the range from 0.1 ppm to 20 ppm. The correlation coefficient was >0.9990 for all analytes of interest.

Gas Chromatography-Flame Ionization Detector (GC-FID) was used for product analysis of the liquid phase; the following chromatographic conditions were employed: carrier gas: He, flow rate: 1 mL min^{-1}, injection volume: 5.0 µL, column oven temperature was initially 40.0 °C and then increased up to 240 °C with the rate of 10 °C per minute, and detector temperature was 250 °C.

X-ray photoelectron spectroscopy (XPS) was performed using a PHI 5000 VersaProbe III spectrometer equipped with an Al-Kα X-ray source (hν = 1486.6 eV) to analyze the chemical state of transition elements. The MOF samples were vacuum-dried at room temperature, and the powdered samples were analyzed under an ultra-high vacuum environment.

Brunauer-Emmett-Teller (BET) surface area and pore volume were measured using a BELLSORP MAX II high-performance gas and vapor adsorption system equipped with three microporous ports. For the BET surface area measurement, the MOF sample was prepared through a freeze-drying process. In this method, the MOF was first soaked in benzene, followed by freezing the slurry at -10 °C and drying it gradually under vacuum at the same temperature. Subsequently, the samples were degassed under vacuum at 80 °C for 24 hours prior to measurement.

Scanning Electron Microscope (SEM) analysis was conducted using a Zeiss FE-SEM Ultra Plus 55 operating at 20 kV to study the morphology and chemical composition of the samples. After vacuum drying, a small amount (1-2 mg) of MOF powder was dispersed onto carbon tape for FE-SEM imaging.

Infra-red (IR) spectra of samples were recorded with FT-IR Spectrometer (MS-632). The MOF samples were vacuum dried at 100 °C to remove the moisture, which was then taken inside the glovebox, and a KBr pellet of powder sample was made.

Electron paramagnetic resonance (EPR) measurements were recorded by a Bruker A300-9.5/12/S/W in the X-band region.

2. Synthesis and characterization of bpy-UiO-67 and bpy-UiO-$FeCl_3$

2.1. Synthesis of [2,2'-bipyridine]-5,5'-dicarboxylic acid

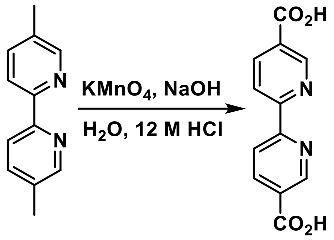

[2,2'-Bipyridine]-5,5'-dicarboxylic acid was synthesized using a modified reported procedure.[1] In a round-bottom flask, 5,5'-dimethyl-2,2'-bipyridyl (0.500 g, 2.74 mmol), sodium hydroxide (0.030 g, 0.75 mmol), and 12 mL of deionized water were combined and stirred at 70 °C. Subsequently, sodium hydroxide (1.48 g, 0.037 mol) was slowly added to the mixture until the pH reached 12. Once the mixture became clear, it was allowed to sit for 1 h. Finely powdered potassium permanganate, $KMnO_4$ (2.140 g, 0.0135 mol) was then added in small portions. The mixture was stirred at 90 °C for 12 h, then cooled to room temperature and filtered. The filtrate was acidified with 12 M hydrochloric acid (HCl), resulting in the formation of a white solid, [2,2'-bipyridine]-5,5'-dicarboxylic acid (0.208 g, 0.85 mmol, 31% yield). The product was analyzed by ^1H NMR spectroscopy. ^1H NMR spectrum (500 MHz, DMSO-d_6): δ 13.55 (s, 2 H), 9.16 (s, 2 H), 8.54 (d, $^3J_{H\text{-}H} = 8.8$ Hz, 2 H), and 8.45 (d, $^3J_{H\text{-}H} = 8.4$ Hz, 2 H).[2]

2.2. Synthesis of bpy-UiO-67 MOF[3]

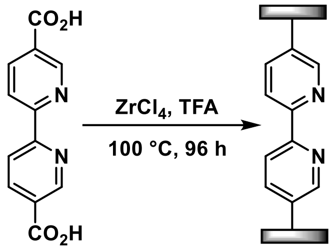

To synthesize bpy-UiO-67 MOF, [2,2'-bipyridine]-5,5'-dicarboxylic acid (0.026 g, 0.106 mmol) and $ZrCl_4$ (0.026 g, 0.112 mmol) were dissolved in 13 mL of DMF. The mixture was sonicated for 30 minutes, after which TFA (0.040 mL, 0.523 mmol) was added. The resulting solution was heated in a sealed 15 mL glass vial at 100 °C for 96 h in an oven. After allowing the reaction mixture to cool to room temperature, the white crystalline solid was isolated by centrifugation, yielding bpy-UiO-67 MOF with a 63% yield. The MOF was thoroughly washed with DMF several times, followed by washing with THF, and then stored in THF at room temperature.

2.3. Synthesis of bpy-UiO-$FeCl_3$

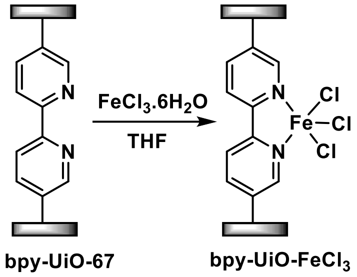

A solution of $FeCl_3.6H_2O$ (0.09 g, 0.34 mmol) in THF was added to the bpy-UiO-67 MOF. The mixture was left overnight with periodic shaking at room temperature. The solid product was then separated by centrifugation and washed 8-10 times with THF, yielding the bpy-UiO-$FeCl_3$ MOF. The bpy-UiO-$FeCl_3$ has 25% solvent weight as analysed by thermogravimetric analysis and 45% iron loading with respect to bpy-moiety of the digested MOF as analyzed by ICP-OES.

Table S1. Inductively Coupled Plasma-Optical Emission Spectrometry (ICP-OES) data of the digested bpy-UiO-$FeCl_3$.

Formula	Zr(ppm)	Fe(ppm)
$Zr_6(\mu_3\text{-}O)_4(\mu_3\text{-}OH)_4(bpy)_6Fe_{6x}Cl_{18x}$	3.24	0.90

<u>**Calculation of Fe loading w.r.t bpy-moiety is as follows:**</u>

Amount of Zr in digested bpy-UiO-$FeCl_3$ MOF = 3.24 ppm

Amount of Fe in digested bpy-UiO-$FeCl_3$ MOF = 0.90 ppm

Mol. weight of Zr = 91.224 g/mol

Mol. weight of Fe = 55.85 g/mol.

Amt. of Zr/ Mol. weight of Zr = 3.24/91.224 = 0.0355

Amt. of Fe/ Mol. weight of Fe = 0.90/55.85 = 0.0161

Therefore, 0.0355 of Zr = 0.0161 of Fe

1 Zr = 1 bpy linker = 0.4539 Fe

Hence, % Fe (% x) = 6/6×0.4539×100

= 45.39% ≈ 45%

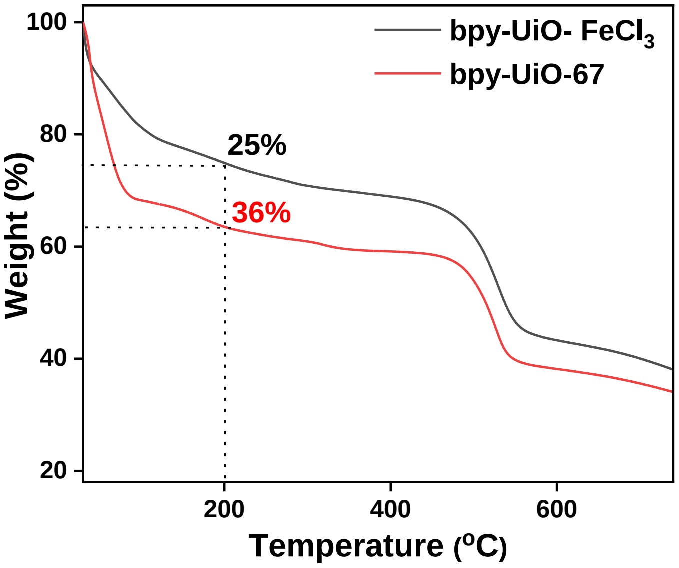

Figure S1. TGA curve of freshly prepared bpy-UiO-67 and bpy-UiO-FeCl$_3$. A solvent weight loss, attributed to THF within the pores, of 36% in bpy-UiO-67 (red) and 25% in bpy-UiO-FeCl$_3$ (black) was observed from 40 °C to 200 °C. The increased weight of metalated MOF is due to the presence of iron chloride moiety within the MOF.

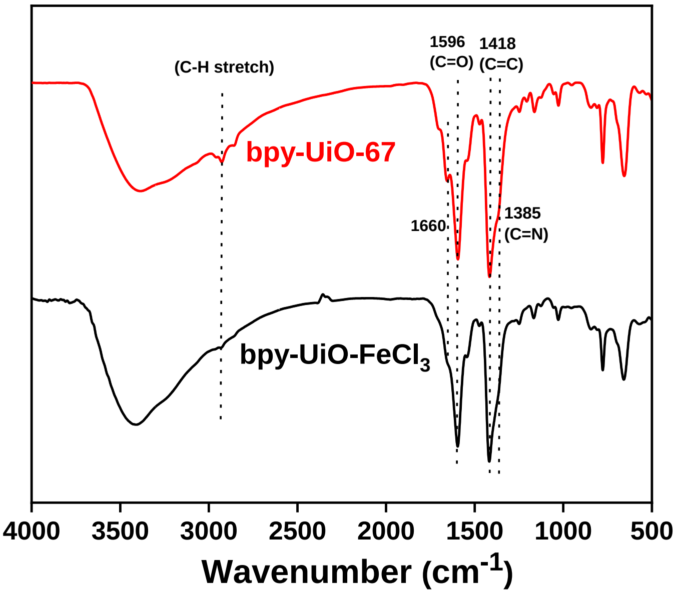

Figure S2. FT-IR spectra (KBr) of freshly prepared bpy-UiO-67 (red) and bpy-UiO-FeCl$_3$ (black). FT-IR spectrum of bpy-UiO-FeCl$_3$ displays a new characteristic absorption peak at 1660 cm^{-1}, indicating a shift of the C=N bond stretching vibration to a lower wavenumber, which suggests that the C=N bond is involved in coordination.

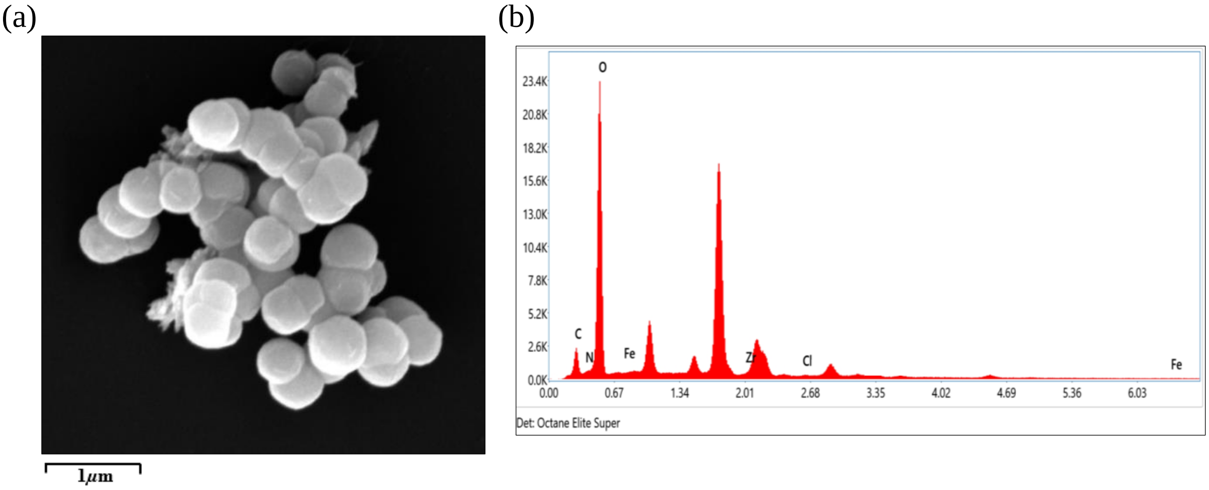

Figure S3. a) SEM image and (b) SEM-EDX analysis of bpy-UiO-$FeCl_3$. SEM image displayed octahedron particles of bpy-UiO-$FeCl_3$ with an average size of 250 nm.

3. Catalytic reactions with bpy-UiO-$FeCl_3$.

3.1. General procedure for bpy-UiO-$FeCl_3$ catalyzed oxidative bromination of arenes. Oxidative bromination of arenes was performed in a 25 mL Schlenk tube. A total of 4 mg of the catalyst bpy-UiO-$FeCl_3$ (0.4 mol% of Fe) was added to 5 mL of the selected solvent. Next, the arene substrate (1 mmol), potassium bromide, KBr (0.13 g, 1.1 mmol), and 0.2 mL (2 mmol) of 30% aqueous hydrogen peroxide (H_2O_2) were added sequentially, with the H_2O_2 introduced dropwise to minimize immediate degradation. The reaction mixture was stirred at a temperature between 30-60 °C for a duration of 30-180 minutes, depending on the desired conversion and selectivity. Once the reaction was complete, the mixture was allowed to cool to room temperature. The solid catalyst was then filtered and dried. To the filtrate, saturated sodium bicarbonate solution was added, and the organic layer was extracted. Anhydrous sodium sulphate was used to dry the organic layer and solvent was evaporated under reduced pressure. The resulting product was analyzed using gas chromatography coupled with mass spectrometry (GC-MS) for identification and flame ionization detection (GC-FID) for quantification. The products were purified by column chromatography using a mixture of ethyl acetate and petroleum benzene and subsequently analyzed by ^1H and ^{13}C NMR spectroscopy.

3.2. A typical procedure for bpy-UiO-$FeCl_3$ catalyzed oxidative bromination of aniline. In a 25 mL Schlenk tube, bpy-UiO-$FeCl_3$ (4 mg, 0.4 mol% of Fe) was added to 5 mL of acetonitrile (CH_3CN). Sequentially, aniline (1 mmol), potassium bromide, KBr (0.13 g, 1.1 mmol), and 0.2 mL (2 mmol) of 30% aqueous H_2O_2 were added. The hydrogen peroxide solution was introduced dropwise to minimize immediate degradation of the reactants. The reaction mixture was stirred at a temperature around 50 °C for 120 minutes. After completing the reaction, the mixture was allowed to cool to room temperature. The solid catalyst was filtered out and dried. To the remaining liquid, a saturated sodium bicarbonate solution was added, and the organic layer was extracted. Anhydrous sodium sulfate was used to dry the organic layer, and the solvent was evaporated under reduced pressure. The resulting product was analyzed using GC-MS for product identification and GC-FID for quantification. The products were purified by column chromatography using a mixture of ethyl acetate and petroleum benzene and subsequently analyzed by ^{1}H and ^{13}C NMR spectroscopy.

Table S2. Bpy-UiO-FeCl$_3$ catalyzed oxidative bromination of aniline.[a]

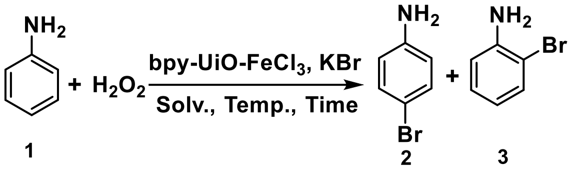

Entry No.	H_2O_2 (mmol)	Brominating agent (mmol)	Temp. (°C)	Time (h)	Solvent	% Conv. of 1	%Yield of 2[b] (2:3)
1	2	KBr (1.1)	40	2	CH_3CN	84	82 (98:2)
2	2	KBr (1.1)	50	2	CH_3CN	98	95 (97:3)
3	2	KBr (1.1)	60	2	CH_3CN	100	89 (89:11)
4	2	KBr (1.1)	50	1	CH_3CN	72	70 (97:3)
5	2	KBr (1.1)	50	3	CH_3CN	100	92 (92:8)
6	2	KBr (1.1)	50	2	CH_3OH	82	72 (88:12)
7	2	KBr (1.1)	50	2	CH_2Cl_2	84	72 (86:14)
8	-	KBr (1.1)	50	2	CH_3CN	0	0
9	1	KBr (1.1)	50	2	CH_3CN	58	55 (95:5)
10	3	KBr (1.1)	50	2	CH_3CN	99	81 (82:18)
11	2	LiBr (1.1)	50	2	CH_3CN	68	50 (74:26)
12	2	NaBr (1.1)	50	2	CH_3CN	79	64 (81:19)
13	2	KBr (1.0)	50	2	CH_3CN	88	85 (97:3)
14[c]	2	KBr (1.1)	50	2	CH_3CN	78	73 (93:7)
15[d]	-	KBr (1.1)	50	2	CH_3CN	0	0

[a]Reaction conditions: Bpy-UiO-FeCl$_3$ (4 mg, 0.4 mol% of Fe), aniline (1 mmol), solvent (5 mL). [b]Yield was determined by GC-FID. [c]Bpy-UiO-FeCl$_3$ (0.2 mol% of Fe). [d]O_2 (1atm) is used as an oxidizing agent.

Table S3: Control experiments for oxidative bromination of aniline.[a]

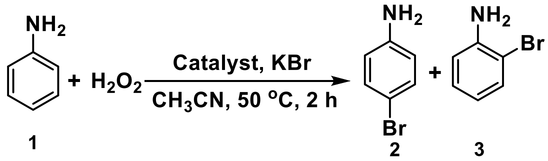

Entry No.	Catalyst	% Conversion of 1	%Yield of 2	2:3
1	Bpy-UiO-$FeCl_3$	98	95	97:3
2	Bpy-UiO-67	0	-	-
3	No catalyst	0	-	-
4	Bpy-UiO-$FeCl_2$	68	63	92:8
5	$FeCl_3.6H_2O$	32	23	71:29
6	Fe nanoparticles	28	19	62:38
7	$FeCl_3$ + bpy (1:1)	33	26	68:32
8[b]	Bpy-UiO-$FeCl_3$	88	85	97:3

[a] Reaction conditions: Catalyst (4.2 μmol of Fe, 0.4 mol% of Fe), aniline (1 mmol), H_2O_2 (2 mmol), KBr (1.1 mmol), CH_3CN (5 mL), 50 °C, 2 h. [b] 1.2 equiv. of tricyclohexylphosphine w.r.t. Fe was added.

Table S4. Comparison of activities of our MOF catalyst with previously reported catalysts for oxidative bromination.

Entry	Catalyst (loading)	Br source	Substrate	Oxidant	Temp., Time	Conv. (%)	Sel. (%)	Ref.
1.	PS-Fe(III)teta complex (3.66% Fe)	KBr	Aniline	H_2O_2	rt, 2.5 h	96	4-bromo aniline (85)	4
2.	$Fe(opbmzl)_2$-Y (0.45% Fe)	KBr	Aniline	H_2O_2	rt, 3 h	84.4	4-bromo aniline (95.6)	5
3.	MNP@DAPN/Au (300mg)	NBS	Aniline		80 °C, 11 h	95	4-bromo aniline (88)	6
4.	$Cu(OAc)_2$	LiBr	Aniline	O_2	80 °C, 4 h	100	4-bromo aniline (80)	7
5.	NH_4VO_3 (10 mol%)	KBr	Anisole	H_2O_2	rt, 24 h		4-bromo aniline (94*)	8
6.	V_2O_5 (3 mol%)	NaBr	Phenol	H_2O_2	rt, 1h	90	4-bromo phenol (69)	9

7.	4Na_2SO_4-2H_2O_2-NaCl adduct	KBr	Aniline	H_2O_2	52 °C, 3 h		4-bromo aniline (90*)	[10]
8.	**Bpy-UiO-$FeCl_3$ (0.4 mol% Fe)**	**KBr**	**Aniline**	**H_2O_2**	**50 °C, 2 h**	**98**	**4-bromo aniline (97)**	**This work**

*NMR-Yield.

3.3. Catalytic testing of Fe nanoparticles. A 3 mL solution of $FeCl_3.6H_2O$ in THF (1.1 mg, 4.01 µmol) was treated with $NaEt_3BH$ (200 µL, 1 M in toluene) for 1 hour. This treatment resulted in the formation of Fe nanoparticles, which settled as a black solid. The nanoparticles were collected by centrifugation and washed thoroughly with THF several times, followed by CH_3CN.

The Fe nanoparticles were then utilized in a reaction setup. In a 25 mL Schlenk tube, the Fe nanoparticles were dispersed in 5 mL of acetonitrile (CH_3CN). Aniline (1 mmol), potassium bromide, KBr (0.13 g, 1.1 mmol), and 30% aqueous hydrogen peroxide (0.2 mL, 2 mmol) were added sequentially. The hydrogen peroxide was introduced dropwise to prevent rapid degradation of the reactants. The reaction mixture was stirred at approximately 50 °C for 120 minutes. After completion of the reaction, the mixture was cooled to room temperature. A saturated sodium bicarbonate solution was added to the mixture, and the organic layer was extracted. The organic phase was dried using anhydrous sodium sulfate, and the solvent was removed under reduced pressure. The resulting product was analyzed by GC-MS for product identification and GC-FID for quantification. The products were purified using column chromatography with a solvent mixture of ethyl acetate and petroleum benzene. The purified products were further characterized by ^1H NMR spectroscopy.

3.4. Test for "heterogeneity" of bpy-UiO-$FeCl_3$ for the oxidative bromination of aniline.

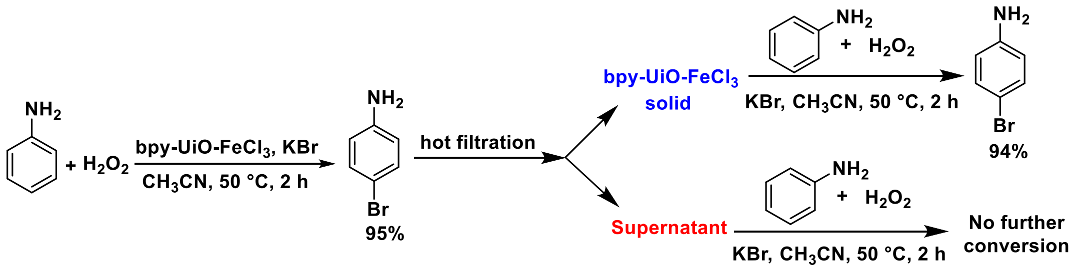

Figure S4. Hot filtration test of bpy-UiO-$FeCl_3$ for the oxidative bromination of aniline.

In a 25 mL Schlenk tube, bpy-UiO-$FeCl_3$ (4 mg, 0.4 mol% of Fe) was dispersed in 5 mL of CH_3CN as the solvent. To this solution, aniline (1 mmol), potassium bromide, KBr (0.13 g, 1.1 mmol), and 30% aqueous hydrogen peroxide (0.2 mL, 2 mmol) were sequentially added. The reaction mixture was stirred at 50 °C for 120 min. After the reaction, the solid MOF catalyst was separated from the hot suspension by filtration and washed thoroughly with CH_3CN. The filtrate was treated with a saturated sodium bicarbonate solution, and the organic layer was extracted. The organic phase was dried over anhydrous sodium sulfate, and the solvent was removed under reduced pressure. Analysis of the resulting supernatant product revealed a 95% yield of 4-bromoaniline.

Two separate reactions were performed using the recovered solid catalyst and the supernatant from the previous reaction to investigate the catalytic activity further. The extracted solid and supernatant were each transferred into individual Schlenk tubes, with 0.1 mL of aniline (1 mmol), 0.34 mL of 30% aqueous hydrogen peroxide (3 mmol), and 5 mL of CH_3CN added to each. The reaction mixtures were heated in an oil bath at 50 °C for 2 h. Analysis using GC-FID revealed that the reaction with the solid MOF catalyst yielded 94% of 4-bromoaniline, while no further conversion of aniline was observed in the reaction using the supernatant. These results confirm that the solid bpy-UiO-$FeCl_3$ MOF functions as the true catalyst for the oxidative bromination of aniline, with no significant contribution from leached Fe species.

3.5. Recycling of bpy-UiO-$FeCl_3$ for the oxidative bromination of aniline.

The recycle and reuse experiment was conducted to check the stability of bpy-UiO-$FeCl_3$ catalyst (Table S5). The detailed procedure of recycling experiment given below.

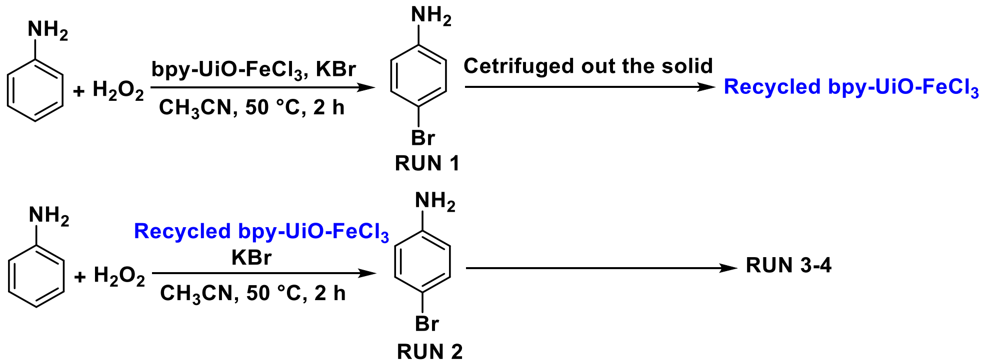

Figure S5. Recycle and reuse of bpy-UiO-$FeCl_3$ for the oxidative bromination of aniline.

In a 25 mL Schlenk tube, bpy-UiO-$FeCl_3$ (4 mg, 0.4 mol% of Fe) was mixed with 5 mL of acetonitrile (CH_3CN) as the solvent. To this solution, aniline (1 mmol), potassium bromide, KBr (0.13 g, 1.1 mmol), and 30% aqueous hydrogen peroxide (0.2 mL, 2 mmol) were sequentially added. The reaction mixture was stirred at 50 °C for 2 h. After the reaction, the solid MOF catalyst was separated from the suspension by filtration and washed thoroughly with CH_3CN. The filtrate was treated with a saturated sodium bicarbonate solution, and the organic layer was extracted. The organic phase was dried over anhydrous sodium sulfate, and the solvent was removed under reduced pressure. Analysis of the resulting product revealed a 95% yield of 4-bromoaniline. The solid MOF was then recycled.

The recovered MOF-catalyst was again added to the Schlenk tube. Aniline (1 mmol), KBr (0.13 g, 1.1 mmol), and 30% aqueous H_2O_2 (0.2 mL, 2 mmol) in 5 mL CH_3CN were added to the Schlenk tube. The reaction mixture was stirred at 50 °C for 2 h. After the reaction, the solution was analyzed in the same way as mentioned previously in run 1. The recycling and reuse experiments were performed up to 3 times in total.

Table S5. %GC-Yield of 4-bromoaniline and the leaching of Fe and Zr at various runs of the recycling of bpy-UiO-FeCl$_3$ in the oxidative bromination of aniline.

Run	Time	%GC-Yield (4-bromoaniline)	%Leaching (Fe, Zr)
Run-1	2 h	95	0.02, 0.6
Run-2	2 h	94	
Run-3	2 h	92	0.08, 1.5
Run-4	2 h	91	

3.6. Radical scavenging experiment.

To investigate the role of any •OH in the bpy-UiO-FeCl$_3$ catalyzed oxidative bromination of aniline, catalysis have been performed in the presence of radical scavengers such as Na_2SO_3, and *tert*-butyl alcohol (TBA).

3.6.1. Radical scavenging experiment using Na_2SO_3 as the radical scavenger. Solid bpy-UiO-FeCl$_3$ (4 mg, 0.4 mol% of Fe) was dissolved in 5 mL of CH_3CN and transferred into a 25 mL Schlenk tube, which was placed in an oil bath maintained at 50 °C. To this, 5 mmol of Na_2SO_3 was added as a radical scavenger, followed by aniline (1 mmol), KBr (0.13 g, 1.1 mmol), and 30% aqueous H_2O_2 (0.2 mL, 2 mmol). After 2 h, the solid MOF catalyst was separated from the reaction mixture by filtration and thoroughly washed with CH_3CN. The filtrate was treated with a saturated $NaHCO_3$ solution, and the organic layer was extracted. The organic phase was dried over anhydrous sodium sulfate, and the solvent was removed under reduced pressure. The resulting product was analyzed using GC-FID.

3.6.2. Radical scavenging experiment using *tert*-butyl alcohol (TBA) as the radical scavenger. Solid bpy-UiO-$FeCl_3$ (4 mg, 0.4 mol% of Fe) was dissolved in 5 mL of CH_3CN and transferred into a 25 mL Schlenk tube, which was placed in an oil bath maintained at 50 °C. To this, 5 mmol of *tert*-butyl alcohol (TBA) was added as a radical scavenger, followed by aniline (1 mmol), KBr (0.13 g, 1.1 mmol), and 30% aqueous H_2O_2 (0.2 mL, 2 mmol). After 2 h, the solid MOF catalyst was separated from the reaction mixture by filtration and thoroughly washed with CH_3CN. The filtrate was treated with a saturated $NaHCO_3$ solution, and the organic layer was extracted. The organic phase was dried over anhydrous sodium sulfate, and the solvent was removed under reduced pressure. The resulting product was analyzed using GC-FID.

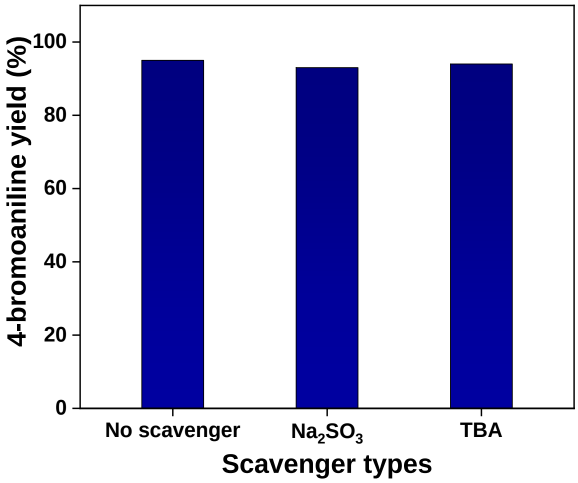

Figure S6. Radical scavenger tests. Reaction conditions: bpy-UiO-$FeCl_3$ (0.4 mol% of Fe), aniline (1 mmol), KBr (1.1 mmol), H_2O_2 (30%) (2 eq.), 5 mL CH_3CN, 50 °C, 2h, trapping agent (5 mmol).

4. Characterization of the products.

4-bromoaniline (2a).[10] 4-bromoaniline was synthesized with 95% yield according to the general procedure for the oxidative bromination of arenes using aniline (1 mmol), H_2O_2 (2 mmol), KBr (1.1 mmol), bpy-UiO-$FeCl_3$ (0.4 mol% of Fe), acetonitrile (5 mL), 50 °C, 2 h. After 2 h, the combined organic extracts were concentrated in vacuo followed by column chromatography using a mixture of ethyl acetate and petroleum benzene (5:1) as an eluent to yield 4-bromoaniline product. ^1H NMR (400 MHz, $CDCl_3$, ppm): δ 7.22 (d, J = 6.7 Hz, 2H), 6.55 (d, J = 6.7 Hz, 2H), 3.46 (s, 2H). ^{13}C NMR (126 MHz, $CDCl_3$, ppm): δ 145.40, 131.99, 116.71, 110.17.

4-bromo-N,N-dimethylaniline (2b).[11] 4-bromo-N,N-dimethylaniline was synthesized with 96% yield according to the general procedure for the oxidative bromination of arenes using N,N-dimethylaniline (1 mmol), H_2O_2 (2 mmol), KBr (1.1 mmol), bpy-UiO-$FeCl_3$ (4 mg, 0.4 mol% of Fe), acetonitrile (5 mL), 50 °C, 2 h. After 2 h, the combined organic extracts were concentrated in vacuo followed by column chromatography using a mixture of ethyl acetate and petroleum benzene (5:1) as an eluent to yield 4-bromo-N,N-dimethylaniline product. ^1H NMR (300 MHz, $CDCl_3$, ppm): δ 7.30 (d, J = 9.0 Hz, 2 H), 6.59 (d, J = 9.0 Hz, 2 H), 2.93 (s, 6 H). ^{13}C NMR (75 MHz, $CDCl_3$, ppm): δ 149.51, 131.68, 114.11, 108.51, 40.57.

4-bromoanisole (2c).[12] 4-bromoanisole was synthesized with 91% yield according to the general procedure for the oxidative bromination of arenes using anisole (1 mmol), H_2O_2 (2 mmol), KBr (1.1 mmol), bpy-UiO-$FeCl_3$ (0.4 mol% of Fe), acetonitrile (5 mL), 50 °C, 2 h. After 2 h, the combined organic extracts were concentrated in vacuo followed by column chromatography using a mixture of ethyl acetate and petroleum benzene (5:1) as an eluent to yield the product. ^1H NMR (300 MHz, $CDCl_3$, ppm): δ 7.37 (d, J = 8.8 Hz, 2H), 6.78 (d, J = 8.8 Hz, 2H), 3.78 (s, 3H). ^{13}C NMR (50 MHz, $CDCl_3$, ppm): δ 158.6, 132.1, 115.6, 112.7, 55.3.

4-bromophenol (2d).[13] 4-bromophenol was synthesized with 86% yield according to the general procedure for the oxidative bromination of arenes using phenol (1 mmol), H_2O_2 (2 mmol), KBr (1.1 mmol), bpy-UiO-$FeCl_3$ (4 mg, 0.4 mol% of Fe), acetonitrile (5 mL), 50 °C, 2 h. After 2 h, the combined organic extracts were concentrated in vacuo followed by column chromatography using a mixture of ethyl acetate and petroleum benzene (5:1) as an eluent to yield 4-bromophenol product. ^1H NMR (400 MHz, $CDCl_3$, ppm): δ 7.37-7.28 (m, 2H), 6.76-6.66 (m, 2H), 5.25 (s, 1H). ^{13}C NMR (101 MHz, $CDCl_3$, ppm): δ 154.6, 132.4, 117.2, 112.8.

4-bromotoluene (2e).[6] 4-bromotoluene was synthesized with 85% yield according to the general procedure for the oxidative bromination of arenes using toluene (1 mmol), H_2O_2 (2 mmol), KBr (1.1 mmol), bpy-UiO-$FeCl_3$ (4 mg, 0.4 mol% of Fe), acetonitrile (5 mL), 50 °C, 2 h. After 2 h, the combined organic extracts were concentrated in vacuo followed by column chromatography using a mixture of ethyl acetate and petroleum benzene (5:1) as an eluent to yield the product. ^1H NMR (500 MHz, $CDCl_3$, ppm): δ 7.42 (d, J = 8.50 Hz, 2H), 7.10 (d, J = 8 Hz, 2H), 2.36 (s, 3H). ^{13}C NMR (125 MHz, $CDCl_3$, ppm): δ 136, 131, 130, 119, 20.9.

Bromobenzene (2f).[6] Bromobenzene was synthesized with 41% yield according to the general procedure for the oxidative bromination of arenes using benzene (1 mmol), H_2O_2 (2 mmol), KBr (1.1 mmol), bpy-UiO-$FeCl_3$ (4 mg, 0.4 mol% of Fe), acetonitrile (5 mL), 50 °C, 10 h. After 10 h, the combined organic extracts were concentrated in vacuo followed by column chromatography using a mixture of ethyl acetate and petroleum benzene (5:1) as an eluent to yield bromobenzene product. ^{1}H NMR (500 MHz, $CDCl_3$, ppm): δ 7.56-7.54 (d, J = 7.5 Hz, 2H), 7.35-7.26(m, 3H). ^{13}C NMR (125 MHz, $CDCl_3$, ppm): δ 132, 130.5, 127.3, 123.

2-bromo-4-methylaniline (2i).[14] 2-bromo-4-methylaniline was synthesized with 71% yield according to the general procedure for the oxidative bromination of arenes using 4-methylaniline (1 mmol), H_2O_2 (2 mmol), KBr (1.1 mmol), bpy-UiO-$FeCl_3$ (4 mg, 0.4 mol% of Fe), acetonitrile (5 mL), 50 °C, 2 h. After 2 h, the combined organic extracts were concentrated in vacuo followed by column chromatography using a mixture of ethyl acetate and petroleum benzene (5:1) as an eluent to yield the product. ^{1}H NMR (500 MHz, $CDCl_3$, ppm): δ 7.24 (s, 1H), 6.92 (d, J = 8.05 Hz,1H), 6.68 (d, J = 8.05 Hz,1H), 3.93 (br, 2H), 2.23 (s, 3H).

2-bromo-1,4-dimethylbenzene (2j).[15] 2-bromo-1,4-dimethylbenzene was synthesized with 70% yield according to the general procedure for the oxidative bromination of arenes using 1,4-dimethylbenzene (1 mmol), H_2O_2 (2 mmol), KBr (1.1 mmol), bpy-UiO-$FeCl_3$ (4 mg, 0.4 mol% of Fe), acetonitrile (5 mL), 50 °C, 2 h. After 2 h, the combined organic extracts were concentrated in vacuo followed by column chromatography using a mixture of ethyl acetate and petroleum benzene (5:1) as an eluent to yield 2-bromo-1,4-dimethylbenzene product. ^{1}H NMR (90 MHz, $CDCl_3$, ppm): δ 82.0(s,3H), 2.1(s,3H), 6.45(d, H), 7.05(d, H), 6.65(s, H).

4-bromo-1,2-dimethylbenzene (2k).[15] 4-bromo-1,2-dimethylbenzene was synthesized with 72% yield according to the general procedure for the oxidative bromination of arenes using 1,2-dimethylbenzene (1 mmol), H_2O_2 (2 mmol), KBr (1.1 mmol), bpy-UiO-$FeCl_3$ (4 mg, 0.4 mol% of Fe), acetonitrile (5 mL), 50 °C, 2 h. After 2 h, the combined organic extracts were concentrated in vacuo followed by column chromatography using a mixture of ethyl acetate and petroleum benzene (5:1) as an eluent to yield 4-bromo-1,2-dimethylbenzene product. ^{1}H NMR (90 MHz, $CDCl_3$, ppm): δ 82.1(s, 3H), 2.4(s, 3H), 7.1-7.45(m, 3H).

4-bromo-2-iodoaniline (2l).[16] 4-bromo-2-iodoaniline was synthesized with 57% yield according to the general procedure for the oxidative bromination of arenes using 2-iodoaniline

(1 mmol), H_2O_2 (2 mmol), KBr (1.1 mmol), bpy-UiO-$FeCl_3$ (4 mg, 0.4 mol% of Fe), acetonitrile (5 mL), 50 °C, 2 h. After 2 h, the combined organic extracts were concentrated in vacuo followed by column chromatography using a mixture of ethyl acetate and petroleum benzene (5:1) as an eluent to yield 4-bromo-2-iodoaniline product. ^{1}H NMR (400 MHz, $CDCl_3$, ppm): δ 7.73 (d, J = 2.4 Hz, 1H), 7.22 (dd, J1 = 8.4 Hz, J2 = 2.0 Hz, 1H), 6.92 (d, S7 J = 8.8 Hz, 1H), 4.10 (s, 2H). ^{13}C NMR (400 MHz, $CDCl_3$, ppm): δ 146.1, 140.5, 132.2, 115.7, 110.0, 84.2.

4-bromo-1,2-dimethoxybenzene (2m). 4-bromo-1,2-dimethoxybenzene was synthesized with 62% yield according to the general procedure for the oxidative bromination of arenes using 1,2-dimethoxybenzene (1 mmol), H_2O_2 (2 mmol), KBr (1.1 mmol), bpy-UiO-$FeCl_3$ (4 mg, 0.4 mol% of Fe), acetonitrile (5 mL), 50 °C, 2 h. After 2 h, the combined organic extracts were concentrated in vacuo followed by column chromatography using a mixture of ethyl acetate and petroleum benzene (5:1) as an eluent to yield 4-bromo-1,2-dimethoxybenzene product. ^{1}H NMR (400 MHz, DMSO, ppm): δ 7.09 (d, J = 2.0 Hz, 1 H), 7.05 (dd, J = 8.6, 2.0 Hz, 1 H), 6.9 (d, J = 8.6 Hz, 1 H), 3.76 (s, 3 H), 3.73 (s, 3 H). ^{13}C NMR (100 MHz, DMSO, ppm): δ 150.3, 148.8, 123.5, 115.3, 113.8, 112.3, 56.2, 56.0.

4-bromo catechol (2n).[17] 4-bromo catechol was synthesized with 68% yield according to the general procedure for the oxidative bromination of arenes using catechol (1 mmol), H_2O_2 (2 mmol), KBr (1.1 mmol), bpy-UiO-$FeCl_3$ (4 mg, 0.4 mol% of Fe), acetonitrile (5 mL), 50 °C, 2 h. After 2 h, the combined organic extracts were concentrated in vacuo followed by column chromatography using a mixture of ethyl acetate and petroleum benzene (5:1) as an eluent to yield 4-bromo catechol product. ^{1}H NMR (400 MHz, CD_3OD, ppm): δ 6.66 (1 H, d, J=8.5 Hz), 6.77 (1 H, dd, J=8.4, 2.3 Hz), 6.89 (1 H, d, J=2.3 Hz). ^{13}C NMR (100 MHz, CD_3OD, ppm): δ 112.0, 117.8, 119.5, 123.6, 146.1, and 147.8.

4-bromo-3-methylaniline (2o).[18] 4-bromo-3-methylaniline was synthesized with 66% yield according to the general procedure for the oxidative bromination of arenes using 3-methylaniline (1 mmol), H_2O_2 (2 mmol), KBr (1.1 mmol), bpy-UiO-$FeCl_3$ (4 mg, 0.4 mol% of Fe), acetonitrile (5 mL), 50 °C, 2 h. After 2 h, the combined organic extracts were concentrated in vacuo, followed by column chromatography using a mixture of ethyl acetate and petroleum benzene (5:1) as an eluent to yield 4-bromo-3-methylaniline product. ^{1}H NMR (400 MHz, $CDCl_3$, ppm): δ 7.28 (d, J = 8.4 Hz, 1H), 6.59 (d, J = 2.4 Hz, 1H), 6.42 (dd, J = 2.4 Hz, J = 8.4

Hz, 1H), 3.60 (br s, 2H), 2.32 (s, 3H). ^{13}C NMR (126 MHz, $CDCl_3$, ppm): δ 145.6, 138.4, 132.7, 117.5, 114.3, 113.0, 22.8.

1-bromo-2,4-dimethylbenzene (2p).[19] 1-bromo-2,4-dimethylbenzene was synthesized with 67% yield according to the general procedure for the oxidative bromination of arenes using 1,3-dimethylbenzene (1 mmol), H_2O_2 (2 mmol), KBr (1.1 mmol), bpy-UiO-$FeCl_3$ (4 mg, 0.4 mol% of Fe), acetonitrile (5 mL), 50 °C, 2 h. After 2 h, the combined organic extracts were concentrated in vacuo followed by column chromatography using a mixture of ethyl acetate and petroleum benzene (5:1) as an eluent to yield 1-bromo-2,4-dimethylbenzene product. ^{1}H NMR (400 MHz, $CDCl_3$, ppm): δ 7.39 (d, J = 8.1 Hz, 1H), 7.05 (s, 1H), 6.86 (d, J = 8.1 Hz, 1H), 2.36 (s, 3H), 2.27 (s, 3H). ^{13}C NMR (126 MHz, $CDCl_3$, ppm): δ 137.4, 137.0, 132.0, 131.7, 128.1, 121.5, 22.8, 20.8.

5. DFT Calculations. All quantum chemical calculations were done using the density functional theory (DFT) with B3LYP[20,21]/def2-SVP[22] level of theory as implemented in the Gaussian 09 software suite.[23–27] Electronic structure complexes were optimized at the unrestricted level. All calculations were performed in the solvated state and at 323.15 K. The solvent effect was incorporated using a continuum solvation model, SMD[28] taking acetonitrile as the solvent. Each structure was first optimized, and then frequency calculation was performed to confirm its geometry and to obtain the thermochemical data. Internal energies were compared directly after accounting for the difference in the number of coordinated CH_3CN molecules. To reduce the computational costs, a simplified bipyridyl ligand was used in these calculations. All the 3D structures were viewed using Gauss View 5.0 software.

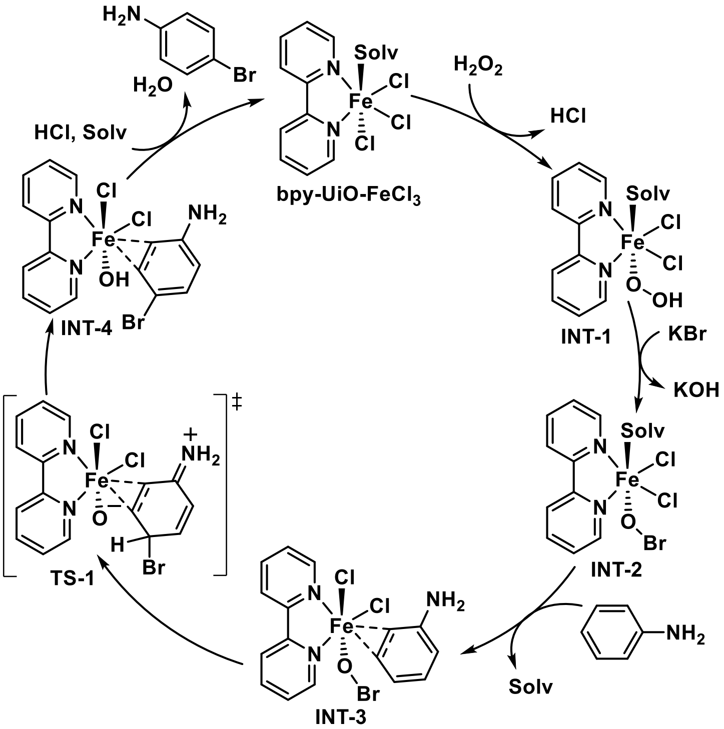

Figure S7. Proposed catalytic cycle of bpy-UiO-$FeCl_3$-catalyzed oxidative bromination of aniline.

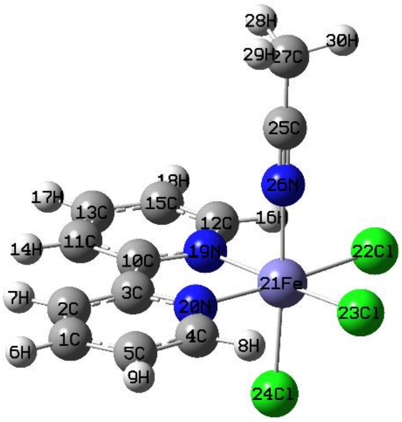

Bpy-UiO-FeCl$_3$

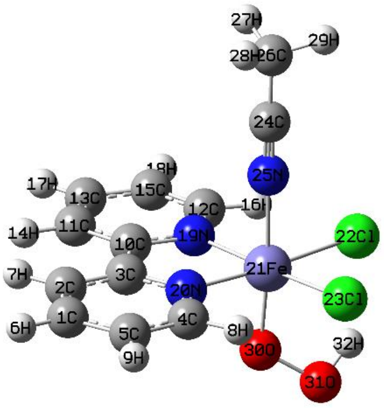

INT-1

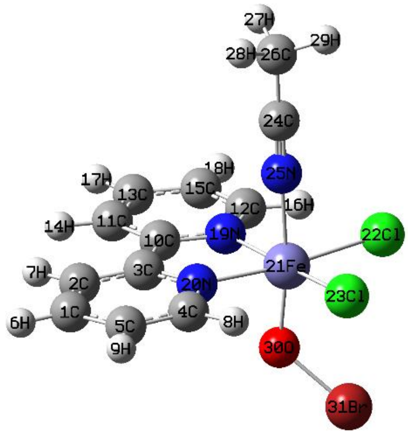

INT-2

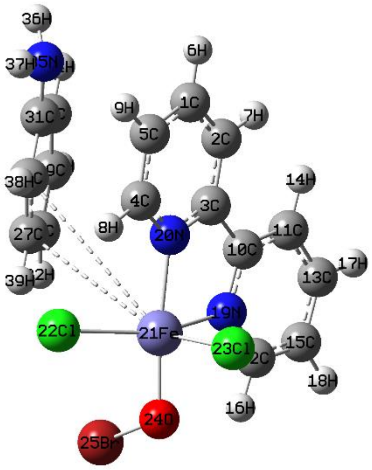

INT-3

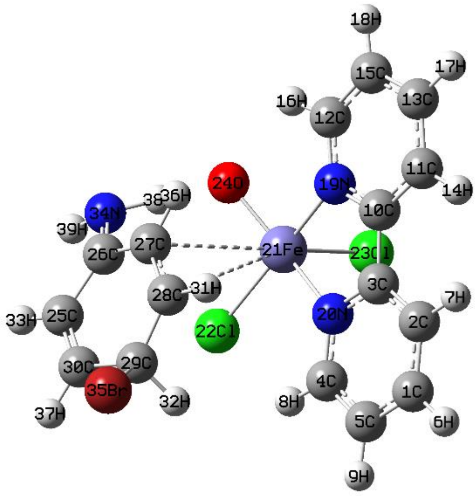

TS-1

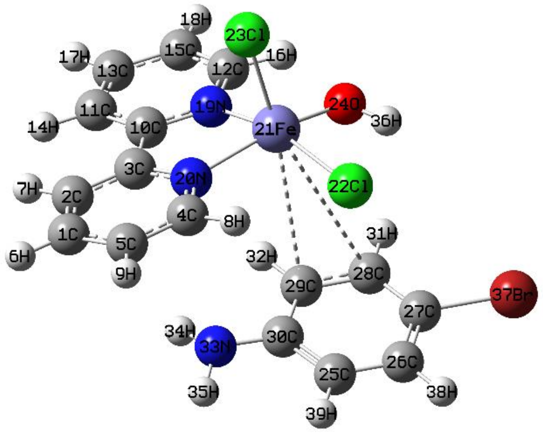

INT-4

Figure S8. DFT-optimized structures of intermediates and transition states of the catalytic cycle in bpy-UiO-FeCl$_3$ catalyzed oxidative bromination of aniline.

5.1. Cartesian coordinates of the DFT-optimized structures.

Cartesian coordinates of bpy-UiO-$FeCl_3$

		Coordinates (Angstroms)		
S.No.	Atoms	X	Y	Z
1	C	-4.205349	-1.182255	0.003445
2	C	-2.815683	-1.285711	-0.035503
3	C	-2.044039	-0.119301	-0.013116
4	C	-3.959023	1.205444	0.085933
5	C	-4.786556	0.084006	0.067247
6	H	-4.823619	-2.082534	-0.011017
7	H	-2.336002	-2.263499	-0.075235
8	H	-4.353862	2.221463	0.135692
9	H	-5.869441	0.215008	0.103369
10	C	-0.571587	-0.102819	-0.028464
11	C	0.227908	-1.248039	-0.103028
12	C	1.313480	1.267847	0.045264
13	C	1.615112	-1.110309	-0.097737
14	H	-0.228432	-2.235633	-0.165145
15	C	2.167509	0.168170	-0.020660
16	H	1.683545	2.292807	0.105793
17	H	2.254429	-1.994154	-0.152961
18	H	3.247534	0.324887	-0.012055
19	N	-0.019171	1.130509	0.040433
20	N	-2.624230	1.102612	0.042663
21	Fe	-1.336679	2.668822	0.146406
22	Cl	0.285240	4.282793	0.208874
23	Cl	-2.993355	4.246447	0.119296
24	Cl	-1.379339	2.419958	2.426015
25	C	-1.247146	2.870808	-2.984625
26	N	-1.284453	2.772708	-1.836255
27	C	-1.173177	2.986212	-4.428721
28	H	-0.257778	2.496363	-4.794262
29	H	-2.050081	2.502313	-4.885113
30	H	-1.155759	4.048916	-4.714841

Cartesian coordinates of INT-1

		Coordinates (Angstroms)		
S.No.	Atoms	X	Y	Z
1	C	-4.212601	-1.186338	0.014907
2	C	-2.823021	-1.292673	-0.028436
3	C	-2.049170	-0.127356	-0.004569
4	C	-3.961455	1.200904	0.101724
5	C	-4.791899	0.081067	0.082202
6	H	-4.832386	-2.085019	-0.001054
7	H	-2.348267	-2.271960	-0.075579
8	H	-4.349608	2.219941	0.153893
9	H	-5.874209	0.212424	0.120941
10	C	-0.576247	-0.109456	-0.027777
11	C	0.227464	-1.252024	-0.103218
12	C	1.304498	1.269670	0.031741
13	C	1.614444	-1.107957	-0.106337
14	H	-0.222281	-2.242511	-0.159210
15	C	2.162934	0.173061	-0.034770
16	H	1.665530	2.298760	0.086782
17	H	2.256695	-1.989040	-0.163415
18	H	3.242126	0.332491	-0.032094
19	N	-0.026944	1.125229	0.033882
20	N	-2.627415	1.094621	0.055870
21	Fe	-1.340141	2.656614	0.152469
22	Cl	0.264846	4.311023	0.222145
23	Cl	-2.999599	4.248398	0.077209
24	C	-1.204984	2.862690	-2.981602
25	N	-1.246420	2.764352	-1.838704
26	C	-1.152995	2.993306	-4.426586
27	H	-0.240542	2.513344	-4.810060
28	H	-2.032424	2.508015	-4.875074
29	H	-1.146155	4.057985	-4.703076
30	O	-1.387962	2.470316	1.962277
31	O	-1.405328	3.662961	2.527693
32	H	-1.428148	3.564700	3.482378

Cartesian coordinates of INT-2

		Coordinates (Angstroms)		
S.No.	Atoms	X	Y	Z
1	C	-4.212601	-1.186338	0.014907
2	C	-2.823021	-1.292673	-0.028436
3	C	-2.049170	-0.127356	-0.004569
4	C	-3.961455	1.200904	0.101724
5	C	-4.791899	0.081067	0.082202
6	H	-4.832386	-2.085019	-0.001054
7	H	-2.348267	-2.271960	-0.075579
8	H	-4.349608	2.219941	0.153893
9	H	-5.874209	0.212424	0.120941
10	C	-0.576247	-0.109456	-0.027777
11	C	0.227464	-1.252024	-0.103218
12	C	1.304498	1.269670	0.031741
13	C	1.614444	-1.107957	-0.106337
14	H	-0.222281	-2.242511	-0.159210
15	C	2.162934	0.173061	-0.034770
16	H	1.665530	2.298760	0.086782
17	H	2.256695	-1.989040	-0.163415
18	H	3.242126	0.332491	-0.032094
19	N	-0.026944	1.125229	0.033882
20	N	-2.627415	1.094621	0.055870
21	Fe	-1.340141	2.656614	0.152469
22	Cl	0.264846	4.311023	0.222145
23	Cl	-2.999599	4.248398	0.077209
24	C	-1.204984	2.862690	-2.981602
25	N	-1.246420	2.764352	-1.838704
26	C	-1.152995	2.993306	-4.426586
27	H	-0.240542	2.513344	-4.810060
28	H	-2.032424	2.508015	-4.875074
29	H	-1.146155	4.057985	-4.703076
30	O	-1.387962	2.470316	1.962277
31	Br	-1.411642	4.096651	2.733299

Cartesian coordinates of INT-3

		Coordinates (Angstroms)		
S.No.	Atoms	X	Y	Z
1	C	-4.092771	-1.027771	-0.479746
2	C	-2.706024	-1.168526	-0.434362
3	C	-1.904110	-0.022917	-0.403971
4	C	-3.780329	1.351858	-0.473819
5	C	-4.639323	0.253482	-0.496201
6	H	-4.735185	-1.910781	-0.503167
7	H	-2.255007	-2.159729	-0.423497
8	H	-4.151322	2.377394	-0.493818
9	H	-5.718097	0.415270	-0.528151
10	C	-0.431562	-0.052879	-0.347341
11	C	0.333956	-1.223289	-0.344684
12	C	1.498246	1.256916	-0.304602
13	C	1.724931	-1.129941	-0.320907
14	H	-0.148911	-2.199220	-0.368409
15	C	2.318457	0.131261	-0.304571
16	H	1.922585	2.259938	-0.301707
17	H	2.335232	-2.035687	-0.324112
18	H	3.402406	0.255605	-0.299019
19	N	0.160827	1.166742	-0.306008
20	N	-2.448560	1.219546	-0.425028
21	Fe	-1.067793	2.740736	-0.509978
22	Cl	-2.693909	4.363466	-0.443083
23	Cl	-1.059581	2.608395	-2.780634
24	O	0.171396	4.072526	-0.727514
25	Br	1.444316	4.736417	0.449685

26	C	-2.430735	2.871710	2.672465
27	C	-1.038863	2.915501	2.678791
28	C	-0.312545	1.881516	3.299707
29	C	-1.003668	0.836056	3.919874
30	C	-2.403919	0.808750	3.929924
31	C	-3.138316	1.822660	3.291294
32	H	0.779593	1.898352	3.296859
33	H	-0.450448	0.036621	4.420400
34	H	-2.934859	-0.006238	4.430420
35	N	-4.536232	1.781252	3.197342
36	H	-4.959727	1.140424	3.854534
37	H	-4.977243	2.686494	3.296310
38	H	-2.973439	3.655355	2.143080
39	H	-0.482124	3.731674	2.204863

Cartesian coordinates of TS-1

		Coordinates (Angstroms)		
S.No.	Atoms	X	Y	Z
1	C	-3.627480	-1.670802	-0.785646
2	C	-2.269695	-1.362330	-0.869853
3	C	-1.866009	-0.031067	-0.723973
4	C	-4.068119	0.658646	-0.415944
5	C	-4.544055	-0.644333	-0.557244
6	H	-3.961947	-2.704434	-0.899235
7	H	-1.536117	-2.148218	-1.047526
8	H	-4.737046	1.500959	-0.229529
9	H	-5.615435	-0.839900	-0.486774
10	C	-0.460708	0.416399	-0.805803
11	C	0.627238	-0.433991	-1.032616
12	C	0.958435	2.268227	-0.686892
13	C	1.912672	0.104223	-1.084575
14	H	0.472047	-1.503865	-1.168520
15	C	2.084014	1.477783	-0.906182
16	H	1.024571	3.348174	-0.542555
17	H	2.771630	-0.546081	-1.263862
18	H	3.071755	1.940644	-0.935851
19	N	-0.273211	1.745334	-0.640400
20	N	-2.764705	0.954670	-0.496612
21	Fe	-1.911752	2.907846	-0.410328
22	Cl	-3.913854	3.831213	0.274011
23	Cl	-2.151189	3.170136	-2.595936
24	O	-1.039966	4.124861	0.107422
25	C	-2.329311	2.664689	5.558337
26	C	-1.555374	1.686706	6.151192
27	C	-0.853102	0.742778	5.362502
28	C	-0.967590	0.809525	3.950731
29	C	-1.741414	1.777280	3.345296
30	C	-2.448012	2.734064	4.138343
31	H	-0.352783	-0.102961	5.831427
32	H	-0.438492	0.077537	3.335780
33	H	-1.826632	1.829703	2.257712
34	H	-2.873940	3.396284	6.160435
35	H	-1.505845	1.627409	7.241440
36	N	-3.215474	3.673355	3.559066
37	H	-3.326680	3.729953	2.543082
38	H	-3.698045	4.361863	4.128759
39	Br	1.807180	1.726822	5.782764

Cartesian coordinates of INT-4

		Coordinates (Angstroms)		
S.No.	Atoms	X	Y	Z
1	C	-4.207565	-1.130812	0.016839
2	C	-2.817468	-1.240457	-0.001980
3	C	-2.042319	-0.075265	0.030158
4	C	-3.953634	1.255389	0.098067
5	C	-4.786794	0.137549	0.067557
6	H	-4.828512	-2.029272	-0.004219
7	H	-2.342628	-2.220842	-0.033414
8	H	-4.339293	2.276630	0.141402
9	H	-5.869920	0.270979	0.086476
10	C	-0.566361	-0.062200	0.027305
11	C	0.228836	-1.211663	-0.046490
12	C	1.321868	1.298602	0.133647
13	C	1.616853	-1.079092	-0.023222
14	H	-0.229430	-2.197406	-0.122156
15	C	2.174113	0.196404	0.072536
16	H	1.690021	2.324826	0.203547
17	H	2.253168	-1.965292	-0.077855
18	H	3.254753	0.347835	0.097474
19	N	-0.009617	1.167705	0.108721
20	N	-2.620187	1.146445	0.078873
21	Fe	-1.328799	2.714937	0.229448
22	Cl	-2.984155	4.323775	0.153190
23	Cl	-1.286307	2.779404	-2.078261
24	O	-0.056362	3.988070	0.235408
25	C	-2.724118	4.750475	2.507883
26	C	-1.389065	5.150227	2.442292
27	C	-0.389839	4.207823	2.200126
28	C	-0.725376	2.864758	2.024601
29	C	-2.060085	2.465103	2.090662
30	C	-3.059590	3.408072	2.331929
31	H	0.062656	2.121878	1.833732
32	H	-2.324849	1.406684	1.952378
33	N	-4.466169	2.986609	2.401233
34	H	-4.700524	2.470638	1.577308
35	H	-4.601775	2.408915	3.206144
36	H	0.565106	4.042167	0.965100
37	Be	1.437809	4.755127	2.109223
38	H	-1.131719	6.179942	2.577790
39	H	-3.490656	5.473658	2.693160

6. X-ray absorption spectroscopic analysis (XAS). X-ray Near-Edge Structure (XANES) and Extended X-ray Absorption Fine Structure (EXAFS) measurements have been carried out at the Energy-Scanning EXAFS beamline (BL-9) at the Indus-2 Synchrotron Source at Raja Ramanna Centre for Advanced Technology (RRCAT), Indore, India.[29] All the measurements were performed at room temperature. This beamline operates in the energy range of 4 keV to 25 keV. The beamline optics consist of a Rh/Pt coated collimating meridional cylindrical mirror and the collimated beam reflected by the mirror is monochromatized by a Si (111) based double crystal monochromator (DCM). The second crystal of the DCM is a sagittal cylindrical crystal which is used for horizontal focusing of the beam while another Rh/Pt coated bendable post mirror facing downward is used for vertical focusing of the beam at the sample position. Two ionization chambers (300 mm length each) have been used for data collection in the transmission mode; one ionization chamber for measuring incident flux, the second one for measuring transmitted flux. For energy calibration, standard metal foils were used. Appropriate gas pressure and gas mixture have been chosen to achieve 10-20% absorption in the first ionization chamber and 70-90% absorption in the second ionization chamber to obtain a better signal-to-noise ratio. Pellets were made from powder samples for recording absorption spectra. Sample powder was mixed homogeneously with cellulose powder in appropriate proportion and pressed (2 Ton) into a 15 mm diameter disc. The amount of the sample was estimated such that to get a reasonable edge jump at a particular absorption edge of the element to be probed. Spectra were collected at the iron K-edge in transmission mode and were calibrated against the reference spectrum of metallic iron (7112 eV). Data were processed using Demeter software.[30] A metallic iron foil standard was used as a reference for energy calibration and was measured simultaneously with experimental samples.

XANES analysis. The oxidation state of Fe within bpy-UiO-$FeCl_3$ were determined by comparison of its pre-edge position with that of $FeCl_3$. The position of the pre-edge of bpy-UiO-$FeCl_3$ (7114.4 eV) aligned well with that of $FeCl_3$ (7114 eV). We, therefore, concluded that Fe ion in bpy-UiO-$FeCl_3$ has +3 oxidation state. Furthermore, a smaller intensity of pre-edge indicates the presence of octahedral geometry.

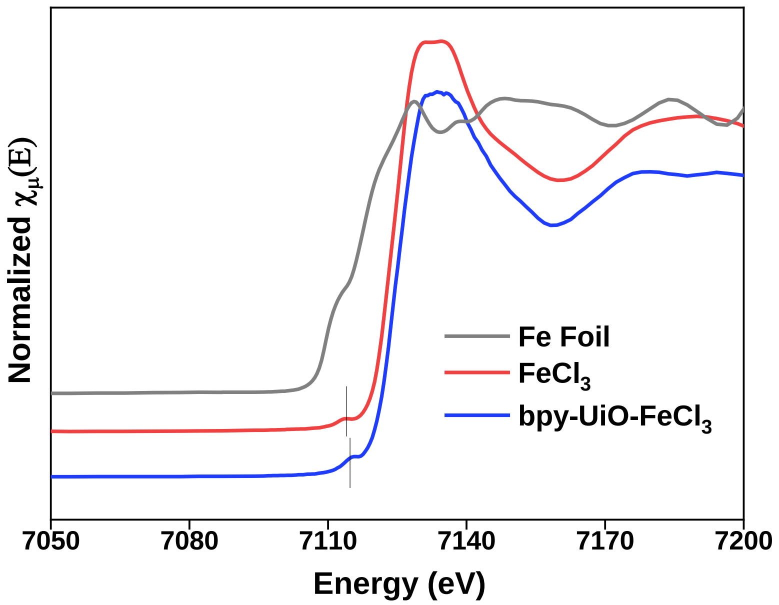

Figure S9. μ(E) XAS spectra of metallic Fe(0) foil (gray), $FeCl_3$ (red) and bpy-UiO-$FeCl_3$ (blue).

EXAFS fitting using DFT optimized structures. The spectra were calibrated against the reference spectra and aligned to the first peak in the smoothed first derivative of the absorption spectrum, the background noise was removed, and the spectra were processed to obtain a normalized unit edge step. The fitting parameters of bpy-UiO-$FeCl_3$ are summarized in Table S6.

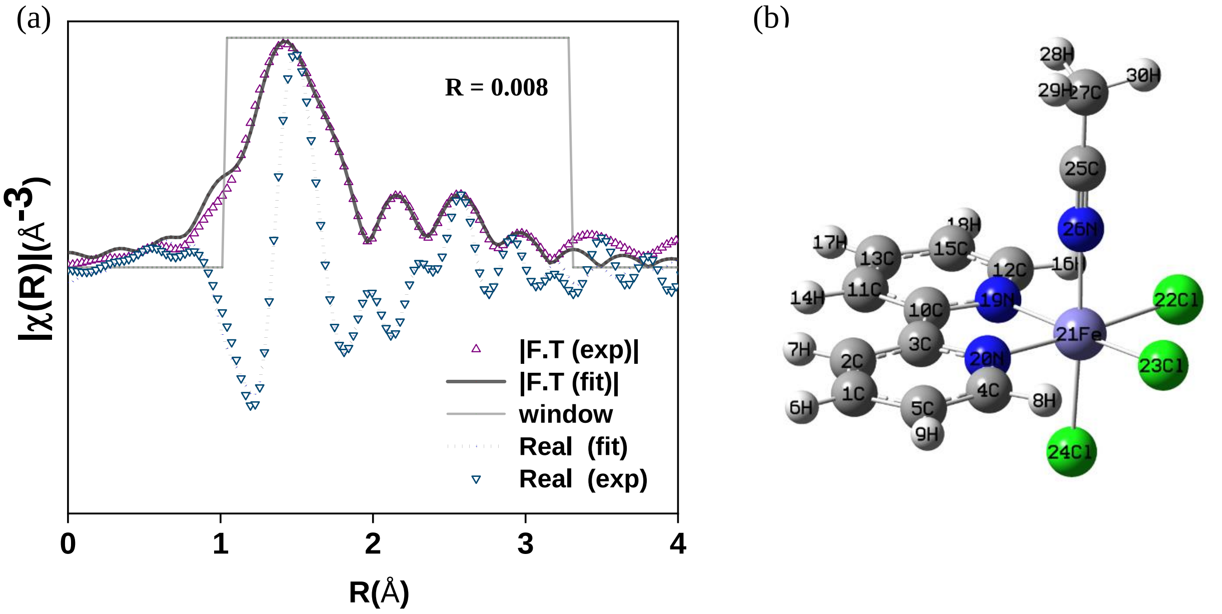

Figure S10. (a) EXAFS spectra and fits of bpy-UiO-$FeCl_3(NCCH_3)$ in the R space from 1 to 3.3 Å. (b) DFT optimized structure of bpy-$FeCl_3(NCCH_3)$.

Table S6. Summary of EXAFS parameters of bpy-UiO-$FeCl_3(NCCH_3)$.

Sample	**bpy-UiO-$FeCl_3(NCCH_3)$**	**Fitting range**	***k* *2*-12.2 $Å^{-1}$** **R 1.0-3.3 Å**
Independent points	15	**R-factor**	0.008
Variables	12	**S_o^2**	0.67
Reduced chi-square	18.39	**ΔE_0(eV)**	-6.24
R(Fe-N20) (Å)	1.90±0.007	**σ^2 (Fe-N20) ($Å^2$)**	0.003±0.001
R(Fe-N19) (Å)	1.90±0.0007	**σ^2 (Fe-N19) ($Å^2$)**	0.003±0.001
R(Fe-N26) (Å)	2.09±0.006	**σ^2 (Fe-N26) ($Å^2$)**	0.003±0.002
R(Fe-Cl22) (Å)	2.19±0.07	**σ^2 (Fe-Cl22) ($Å^2$)**	0.002±0.001
R(Fe-Cl23) (Å)	2.19±0.07	**σ^2 (Fe-Cl23) ($Å^2$)**	0.003±0.002
R(Fe-Cl24) (Å)	2.39±0.006	**σ^2(Fe-Cl24) ($Å^2$)**	0.004±0.003
R(Fe-C20) (Å)	2.77±0.09	**σ^2 (Fe-C20) ($Å^2$)**	0.005±0.003
R(Fe-C19) (Å)	2.80±0.09	**σ^2 (Fe-C19) ($Å^2$)**	0.005±0.003
R(Fe-C25) (Å)	2.92±0.07	**σ^2 (Fe-C25) ($Å^2$)**	0.01±0.005
R(Fe-C4) (Å)	3.06±0.07	**σ^2 (Fe-C4) ($Å^2$)**	0.01±0.005
R(Fe-C12) (Å)	3.06±0.07	**σ^2 (Fe-C12) ($Å^2$)**	0.01±0.005

7. XPS analysis of bpy-UiO-FeCl$_3$.

All the binding energies were corrected with reference to the C1s peak at 284.8 eV. MULTIPAK software was used for peak analysis and de-convolution studies.

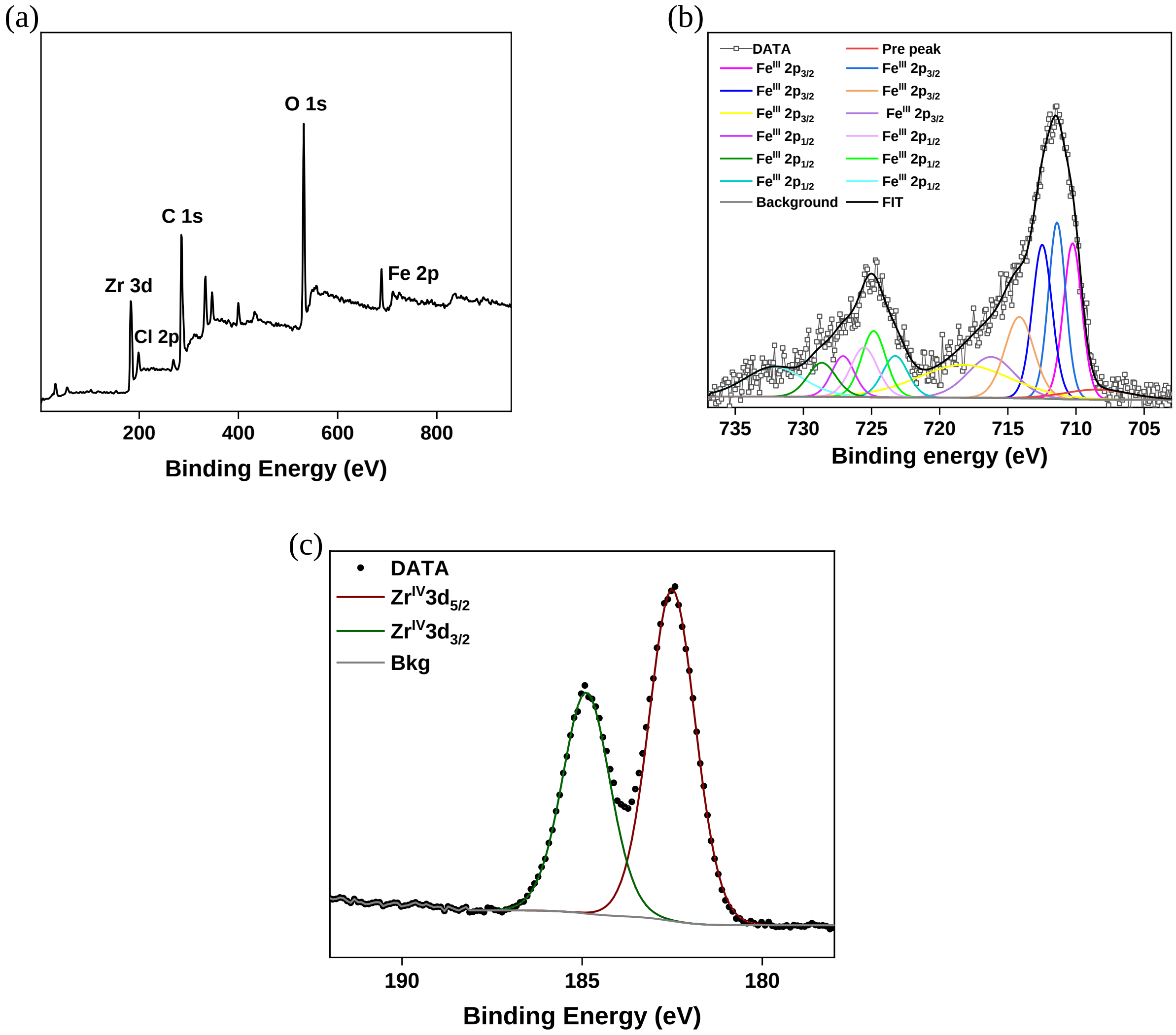

Figure S11. (a) Raw XPS data of bpy-UiO-FeCl$_3$. (b) XPS fitting of iron in bpy-UiO-FeCl$_3$. (c) XPS fitting of zirconium in bpy-UiO-FeCl$_3$.

Table S7. XPS fitting parameters for Fe(III) in bpy-UiO-FeCl$_3$ MOF.

Component	Position (eV)	FWHM (eV)	Area%	Line shape
Fe(III) 2p	710.25	1.5	11.76	GL(30)
Fe(III) 2p	711.39	1.4	12.37	GL(30)
Fe(III) 2p	712.48	1.6	12.32	GL(30)
Fe(III) 2p	714.16	1.7	9.64	GL(30)
Fe(III) 2p	716.23	4.3	7.80	GL(30)

Fe(III) 2p	719.01	5.1	12.47	GL(30)
Fe(III) 2p	723.26	1.9	4.27	GL(30)
Fe(III) 2p	724.84	1.9	6.54	GL(30)
Fe(III) 2p	725.55	2.1	5.42	GL(30)
Fe(III) 2p	727.09	1.9	3.76	GL(30)
Fe(III) 2p	728.65	2.3	3.89	GL(30)
Fe(III) 2p	732.15	4.3	7.07	GL(30)
Fe(III) 2p	708.46	3.7	2.67	GL(30)

(a) (b)

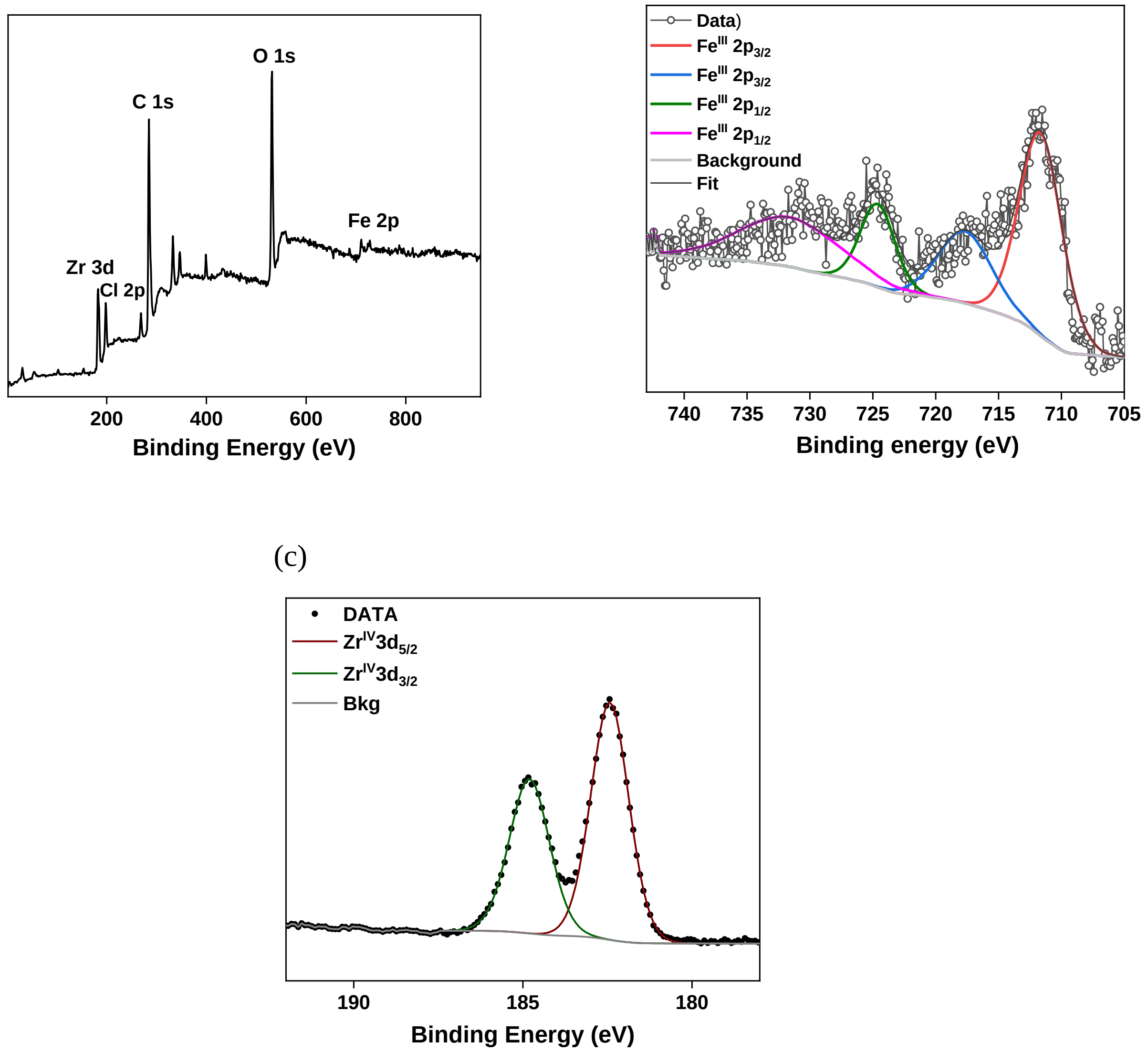

Figure S12. (a) Raw XPS data of bpy-UiO-FeCl$_3$ after catalysis. (b) XPS fitting of iron in bpy-UiO-FeCl$_3$ after catalysis. (c) XPS fitting of zirconium in bpy-UiO-FeCl$_3$ after catalysis.

8. References.

1 L.-J. Zhou, W.-H. Deng, Y.-L. Wang, G. Xu, S.-G. Yin and Q.-Y. Liu, *Inorg. Chem.*, 2016, **55**, 6271–6277.

2 S. Øien, G. Agostini, S. Svelle, E. Borfecchia, K. A. Lomachenko, L. Mino, E. Gallo, S. Bordiga, U. Olsbye, K. P. Lillerud and C. Lamberti, *Chem. Mater.*, 2015, **27**, 1042–1056.

3 Y. Zhao, S. Zhang, M. Wang, J. Han, H. Wang, Z. Li and X. Liu, *Dalton Trans.*, 2018, **47**, 4646–4652.

4 Sk. M. Islam, K. Ghosh, A. S. Roy, N. Salam and T. Chatterjee, *J. Inorg. Organomet. Polym. Mater.*, 2014, **24**, 457–467.

5 S. Eshwar Rao and G. Virupaiah, *J. Chem. Technol. Biotechnol.*, 2017, **92**, 2060–2074.

6 A. Pourjavadi, N. Keshavarzi, S. H. Hosseini and F. M. Moghaddam, *Ind. Eng. Chem. Res.*, 2018, **57**, 12314–12322.

7 L. Menini, J. C. da Cruz Santos and E. V. Gusevskaya, *Adv. Synth. Catal.*, 2008, **350**, 2052–2058.

8 T. Moriuchi, M. Yamaguchi, K. Kikushima and T. Hirao, *Tetrahedron Lett.*, 2007, **48**, 2667–2670.

9 G. Rothenberg and J. H. Clark, *Org. Process Res. Dev.*, 2000, **4**, 270–274.

10 E. M. Gayakwad, K. P. Patel and G. S. Shankarling, *New J. Chem.*, 2019, **43**, 6001–6009.

11 M. Tajbakhsh, R. Hosseinzadeh, H. Alinezhad, S. Ghahari, A. Heydari and S. Khaksar, *Synthesis*, 2011, **2011**, 490–496.

12 F. Mo, J. M. Yan, D. Qiu, F. Li, Y. Zhang and J. Wang, *Angew. Chem. Int. Ed.*, 2010, **49**, 2028–2032.

13 X.-L. Li, R.-Z. Zhang, K.-K. Niu, R.-Z. Dong, H. Liu, S.-S. Yu, Y.-B. Wang and L.-B. Xing, *Chem. Commun.*, 2023, **59**, 13301–13304.

14 J. Lv, Q. Liu, J. Tang, F. Perdih and K. Kranjc, *Tetrahedron Lett.*, 2012, **53**, 5248–5252.

15 C. Venkatachalapathy and K. Pitchumani, *Tetrahedron*, 1997, **53**, 2581–2584.

16 N. Rong, Y. Yuan, H. Chen, C. Yao, T. Li, Y. Wang and W. Yang, *Org. Chem. Front.*, 2021, **8**, 4479–4484.

17 L. Coulombel, L. C. Nolan, J. Nikodinovic, E. M. Doyle and K. E. O'Connor, *Appl. Microbiol. Biotechnol.*, 2011, **89**, 1867–1875.

18 H. Wang, K. Wen, N. Nurahmat, Y. Shao, H. Zhang, C. Wei, Y. Li, Y. Shen and Z. Sun, *Beilstein J. Org. Chem.*, 2012, **8**, 744–748.

19 J. M. Quibell, G. J. P. Perry, D. M. Cannas and I. Larrosa, *Chem. Sci.*, 2018, **9**, 3860–3865.

20 A. D. Becke, *J. Chem. Phys.*, 1993, **98**, 5648–5652.

21 C. Lee, W. Yang and R. G. Parr, *Phys. Rev. B*, 1988, **37**, 785–789.

22 F. Weigend and R. Ahlrichs, *Phys. Chem. Chem. Phys.*, 2005, **7**, 3297.

23 M. Araújo, B. Lasorne, A. L. Magalhães, G. A. Worth, M. J. Bearpark and M. A. Robb, *J. Chem. Phys.*, 2009, **131**, 144301.

24 V. Yempally, S. J. Kyran, R. K. Raju, W. Y. Fan, E. N. Brothers, D. J. Darensbourg and A. A. Bengali, *Inorg. Chem.*, 2014, **53**, 4081–4088.

25 M. Darvish Ganji, S. M. Hosseini-khah and Z. Amini-tabar, *Phys. Chem. Chem. Phys.*, 2015, **17**, 2504–2511.

26 S. Impeng, S. Siwaipram, S. Bureekaew and M. Probst, *Phys. Chem. Chem. Phys.*, 2017, **19**, 3782–3791.

27 S. Canneaux, F. Bohr and E. Henon, *J. Comput. Chem.*, 2014, **35**, 82–93.

28 A. V. Marenich, C. J. Cramer and D. G. Truhlar, *J. Phys. Chem. B*, 2009, **113**, 6378–6396.

29 A. K. Poswal, A. Agrawal, A. K. Yadav, C. Nayak, S. Basu, S. R. Kane, C. K. Garg, D. Bhattachryya, S. N. Jha and N. K. Sahoo, *AIP Conf. Proc.*, 2014, **1591**, 649–651.

30 B. Ravel and M. Newville, *J. Synchrotron Radiat.*, 2005, **12**, 537–541.